TECHNICAL RESEARCH REPORT

*Institute for Systems Research*

# Analysis of Elastoplastic Deformation Observed on Machined Surfaces

*by T-W. Hwang and G.M. Zhang*

*The Institute for Systems Research is supported by the National Science Foundation Engineering Research Center Program (NSFD CD 8803012), Industry and the University*

TR 93-10

# Analysis of Elastoplastic Deformation Observed on Machined Surfaces

Tsu-Wei Hwang and Guangming Zhang
Department of Mechanical Engineering and
Institute for Systems Research
University of Maryland
College Park, Maryland 20742

**Abstract**

In this paper, the study of material removal mechanism is focused on a non-linear quasi-static analysis of the elastoplastic interaction between a single-point cutting tool and the material being cut. An updated Lagrange procedure is applied to solve the large strain elastoplastic deformation problem which generates part of the irregularities observed on machined surfaces. A unique three-dimensional finite element model is developed to simulate the single-point metal cutting process. The effects of cutting parameter settings and workpiece material on the elastoplastic deformation of machined surfaces are investigated. The validity of this analysis is verified by experiments. The results of this analysis can be applied as a surface texture modification model to enhance the accuracy of a computer-aided surface texture simulator, an important part of a computer integrated manufacturing system.

## 1 Introduction

It is clear that surface quality as well as dimensional accuracy are important for the functional requirements of many engineering components and interfaces. It is also evident that the quality of a machined surface is closely related to the machining processes used for producing the part. Therefore, understanding of the mechanism of surface texture formation during machining is compulsory to improve the quality of machined parts.

Metal cutting processes have been studied extensively for a long time. Due to the complexity of the material removal process, it is extremely difficult to have a general model which can interpret the various mechanism taking place at the contact region of the cutting tool and the material being cut. The formation of a machined surface, as mostly observed from a single-point cutting process (such as turning), may at least be affected by three major causes [Shaw 84]: a) the geometry of cutting tool and cutting parameter settings which form the basic shape of a machined surface or the *nominal machined surface*, b) vibration or chattering of the machine tool, caused by the dynamic cutting force variation during machining, which superimposes the trace of tool tip vibratory motion on the nominal machined surface, and c) the elastoplastic interaction between the tool-workpiece interface, which will not only deform the material but also keep residual stresses inside the machined parts.

It is evident that both tool vibration and elastoplastic deformation will cause the irregularities observed on a machined surface. Study of the stability of a machine tool structure to suppress the tool vibration during machining has been very promising in reducing the surface irregularities caused by tool vibration [TlAn 83]. However, the basic mechanism of the elastoplastic process occurred on the tool-workpiece interface has not yet been clearly understood. The research in this area has drawn the most attention from those who have attempted analyses of machining. Most of the research is based on the study of the orthogonal cutting process [ErMe 41]. Their contributions have provided a foundation for the understanding of the basic mechanism of metal cutting processes; however, it is still difficult to explain the surface formation mechanism in metal cutting.

The computer advancement and the development of numerical methods have provided powerful tools for doing research in machining processes. Finite element method is the most prominent one among them. The first finite element analysis for metal cutting was due to Klamecki [Kl 73] who treated the incipient chip formation process using a three-dimensional model. However, the model he used did not examine the formation of a machined surface. Ever since, many other finite element models have been proposed by researchers [Ta. 74, UsSh 82, St. 83, Iw. 84, StCa 85, CaSt 88, Lin 91, Ko. 91]. Unfortunately, all of these models dealt with orthogonal cutting only, which assumes a plane-strain condition for the workpiece material being machined (see Fig. 1), Figure 1b is

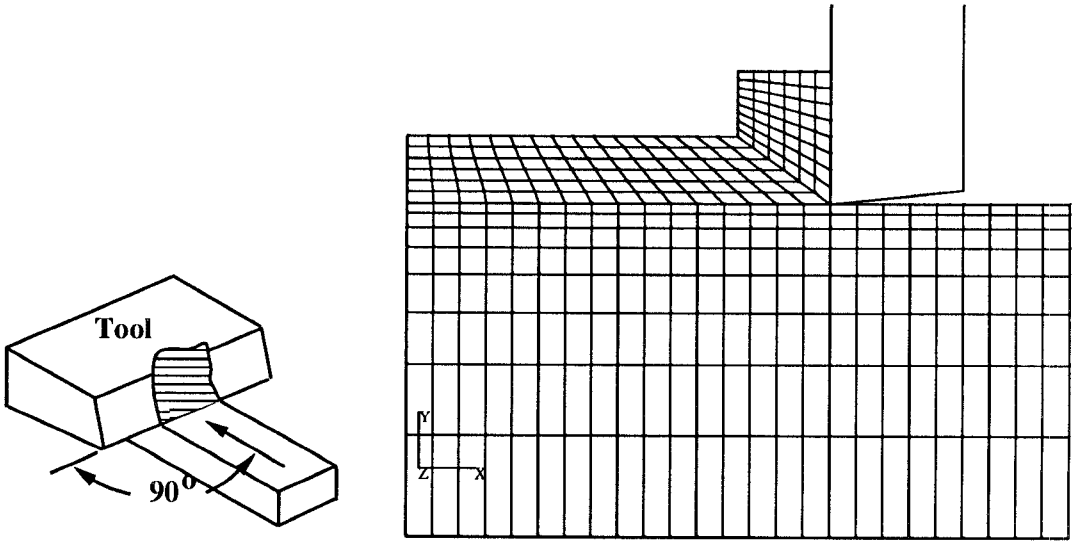


(a) Orthogonal Cutting (b) Finite Element Mesh for Orthogonal Cutting

Figure 1: Orthogonal Cutting Process and Its Finite Element Model

a popular two-dimensional finite element mesh for orthogonal cutting analysis. Although it has been demonstrated by researchers that this two-dimensional model can provide information about the residual stresses underneath the machined surface, it is not capable of explaining the effect of elasoplastic deformation on machined surface textures. It is believed that a three-dimensional finite element model and analysis procedure are more suitable to

reveal the elatoplastic effect on surface texture formation in metal cutting processes.

In the next section, investigation of the tool-workpiece interface observed under cutting processes is described. Based on the investigation, the procedure to analyze such a cutting process using a three-dimensional finite element model is discussed in detail in Section 3. Experimental verification and discussion of results are presented in Section 4 where results from this analysis are compared with those from the turning of steel and aluminum alloy materials. Implications of this research to improve the accuracy of a computer-aided surface texture simulator is discussed in Section 4. Conclusions are summarized in Section 5.

## 2 Investigation of the Tool-Workpiece Contact Area

Traditionally, the movement of the work material and the chip across the faces around the edge of a tool has been treated as a classical friction action where *frictional forces* tend to restrain the chip movement on the tool rake face. However, close studies of the tool-workpiece interface have revealed that this friction action is not what really happened for most metal cutting conditions (especially at high cutting speed) [Tr 91].

Under loading conditions in engineering sliding contact problems, the *real contact* area is very small, often less than one hundredth of the *apparent area* of the contact surfaces. The frictional force is that required to break the bonding force between the molecules on the two *real contact* surfaces. This frictional force is proportional to the normal force between the two surfaces. However, when the normal force on the tool-chip interface is increased to such an extent (as in metal cutting) that the real area of contact is a large proportion of the *apparent contact* area due to plastic deformation, the force required to move one body over another is the frictional force needed to shear the weaker of the two materials across the whole contact area. This force is independent of the normal force when cutting at high speed, but is directly proportional to the area of contact, a relationship totally opposed to that of classical friction theory [BoTa 54].

Figure 2 shows examples of the *real* contact area under three different normal forces. In Fig. 2a, the normal force is the smallest; and the *real* contact area (at points A, B and C) is far less than the apparent contact area. As shown in Fig. 2b, when the normal force increases so does the *real* contact area (at points A', B' and C'). When the normal force is extremely large, the two surfaces are forced almost in complete contact as in Fig. 2c. Consequently, the friction force is no longer independent of the contact area as discussed above.

When cutting at high speed, the just-formed chip tends to stick to the tool rake face [Tr 91]. On the tool flank face, the workpiece material underneath the tool edge is tracked by the tool edge as the tool moves across the newly formed surface. A three dimensional view of a single-point cutting process is schematically shown in Fig. 3 where a very hard cutting tool with a nose radius ($R$) moves into an uncut chip cross section (determined by the tool geometry and cutting parameter settings) of the workpiece material. The material just in front of the cutting tool edge experiences a large compressive stress and, therefore, is pushed back with large strain. When the cutting edge pushes further, it leads to the fracture of the work material, and chip separates from the workpiece along the cutting edge.

It is perceived that the contact deformation of the workpiece and tool material, both

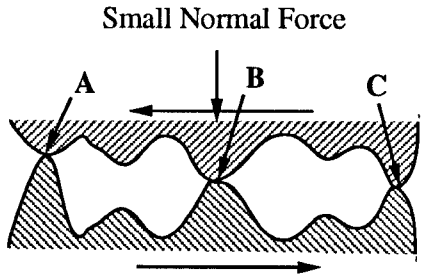


(a) Sliding Contact under Small Normal Force

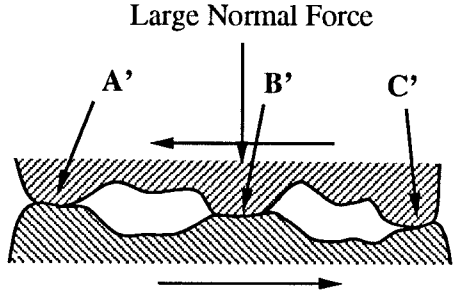


(b) Sliding Contact under Large Normal Force

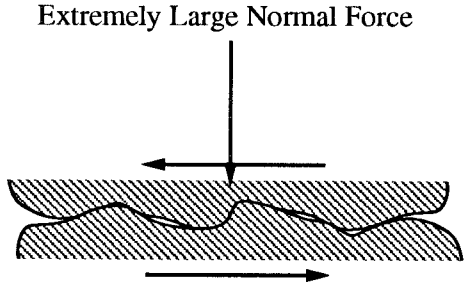


(c) Sliding Contact under Extremely Large Normal Force

Figure 2: Examples of Sliding Contact under Different Normal Forces

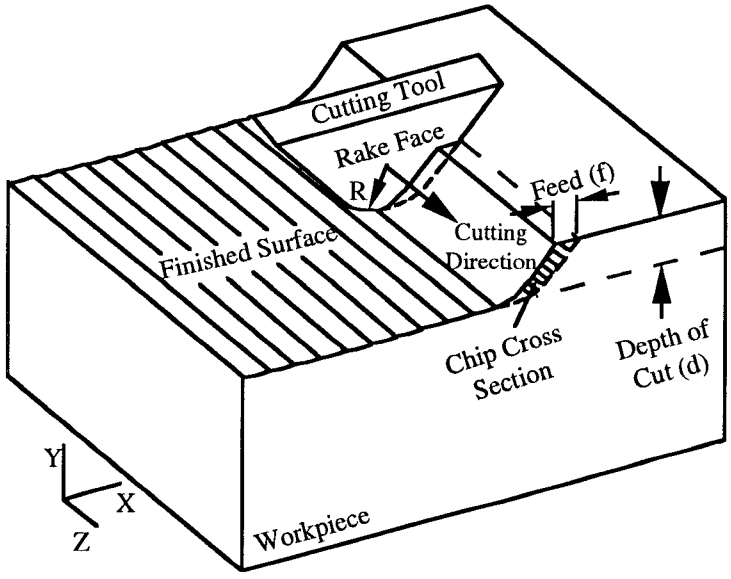


Figure 3: Three-Dimensional Representation of a Single-Point Cutting Process

elastic and plastic, develops during machining. Because the hardness of the workpiece material is relatively low with respect to the hardness of the tool material, the contact deformation is mostly on the workpiece side. Depending on the stress distributed on the contact area, plastic deformation is superior to elastic deformation due to the high pressure exerted by the cutting tool at certain points of the workpiece surface and its sub-layer elements. A severe work hardening of the workpiece develops when the tool moves across the contact area during machining. As a result, these points will sustain the tool path trajectory with little distortion caused by the recovery of the plastic deformation. On the other hand, those points on the surface exerted by lower cutting pressure present elastic deformation. The recovery from the elastic deformation is more significant at these points as the cutting tool travels along the surface. Consequently, the surface is somewhat distorted due to the elastic-plastic deformation in the recovery process.

Observations of the temperature effect on the stress-strain distribution in the tool-work and tool-chip interfaces have also been made by researchers. It is well known that most of the heat resulting from the work done on the shear plane to form the chip remains in the chip and is carried away with it, while a small amount but variable percentage is conducted into the workpiece and raises its temperature [Kr 66, Shaw 84, Tr 91]. Figure 4 shows that the cutting tool has the highest temperature distribution and the workpiece has the lowest temperature distribution under different cutting speed. On the other hand, the temperature

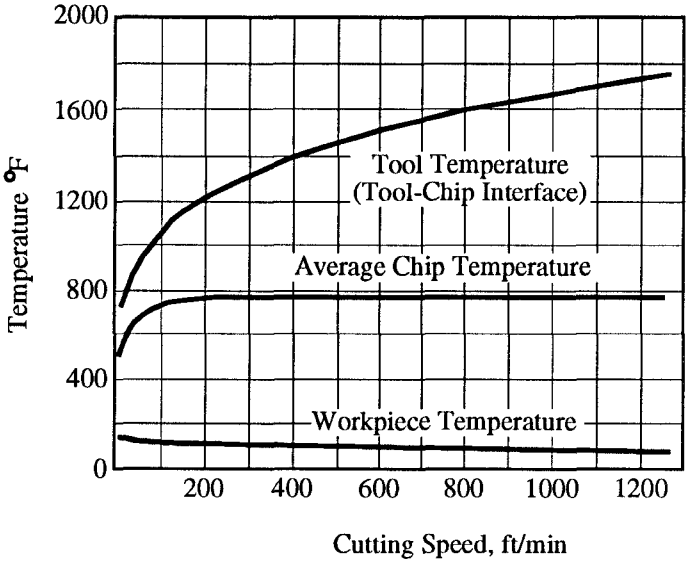


Figure 4: A Typical Temperature Distribution in Metal Cutting
(from [Kr 66])

effect on the chip tends to be compensated by the effects due to the strain rate increased under the same cutting condition as has been observed by researchers [Shaw 84, Tr 91]. Actually, the temperature effect tends to have more effect on the tool life than on the workpiece [Tr 91]. If the cutting temperature is properly controlled during cutting process (e.g., using cutting fluid to dissipate the heat generated during machining), it can be treated as a non-dominant factor in the elastoplastic deformation process on the machined workpiece

material [Lin 91].

From the above investigation of the tool-workpiece interface, it becomes apparent that the development of a closed form solution to explain the elastoplastic deformation process observed on the machined surface is extremely difficult due to the complex deformation phenomena. Therefore, numerical techniques, such as the finite element method, may provide a good alternative for solving such a problem. Since our purpose is to investigate the effects of elastoplastic deformation process on the machined surfaces, this research is aimed at developing a three-dimensional finite element model which can account for the essential features observed in the metal cutting processes and can provide closer approximation to the actual deformed shape of a machined surface. The effects of different cutting conditions (feed rate and depth of cut) on the deformation process are also examined by a three-dimensional finite element model.

# 3 Three-Dimensional Finite Element Modeling

## 3.1 Major Features and Assumptions of the Model

Based on the need from the investigation mentioned in the previous Section, a three-dimensional finite element mesh is generated as shown in Fig. 5. The major features and assumptions of the generated meshes are:

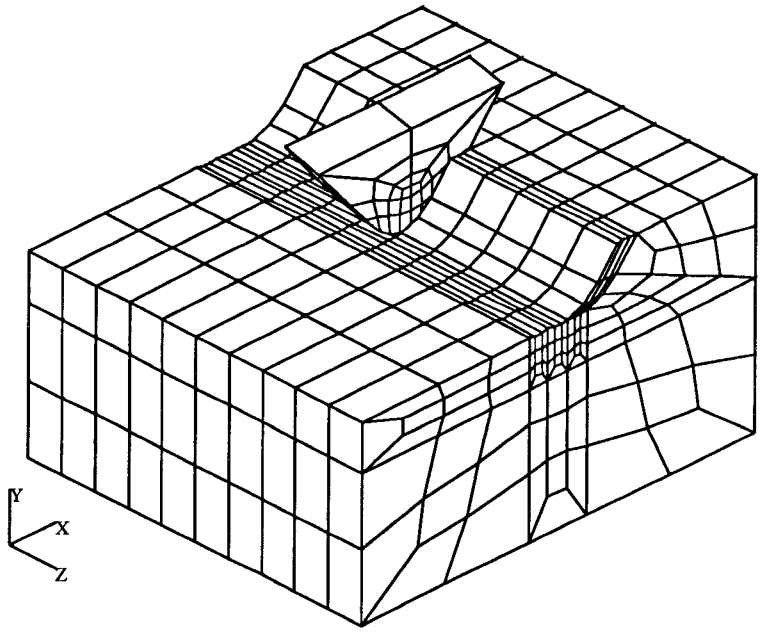


Figure 5: Three-Dimensional Finite Element Model

1. The tool material is treated as a rigid body moving across the workpiece material along a predefined tool path. Most of the cutting tool materials used for machining

have much higher hardness values than those of the workpiece materials. For example, the hardness of a tungsten carbide tool insert is usually in the range of (1800 - 3200 BHN ) compared with that of a low carbon steel workpiece material which is around 140 BHN. It is reasonable to make such an assumption (tool is a rigid body) that the computer resource can be reserved for other features without sacrificing the accuracy of calculation.

2. In Fig. 5, there are 885 isoparametric, eight-node three-dimensional brick type of elements in the workpiece material model. The size of the element is based on a criterion such that the aspect ratio (e.g., the ratio of the larger dimension, say in the $X$ direction, to the smaller dimension, say in the $Y$ direction, of an element) of each element should not exceed a fixed upper limit [MARC 91]. Among the 885 elements, the interested area is near the tool path as shown in the middle part of the model. Therefore, finer meshes are necessary in this area to take the surface deformation during cutting into account.

3. Except the surface on top of the workpiece model, the nodes on the bounding surfaces of the workpiece are constrained in all the six degrees of freedom. This can be viewed as if a chunk of the workpiece, on which the tool is passing by, is *extracted* from its surrounding material. It is a common practice to assume that the boundaries of this chunk, *remote* from the tool-work interface, can be treated as deformation free when the material is being cut [ZiGo 74]. As shown in Fig. 5, the size of this chunk, depending on the geometry and size of the tool-work contact area, is chosen to be 4.69 $mm$ in the $X$ direction, 2.48 $mm$ in the $Y$ direction, and 4.00 $mm$ in the $Z$ direction, which can account for the cases applied in this study.

4. Adhesion occurred on tool-chip interface is assumed for the analysis. As mentioned earlier that the most important conclusion from the observation of the tool-work contact area is that the tool-chip interface may be under adhesion condition instead of friction if high cutting speed is used. This assumption yields that when the cutting tool moves across the workpiece, the contact between the tool and material is dominated by the normal force exerted on the interface of the tool and chip. This condition can be simulated by a special *contact* option under the finite element solution phase as will be discussed later.

5. As discussed in Section 2, the temperature effect can be excluded from this analysis since most of the concern on temperature is related to its effect on cutting tool life rather than on the workpiece material [Tr 91]. By disregarding the temperature effect, it alleviates the needs to a) find out the relation between the temperature variation and the stress-strain curve for different materials, and b) build a temperature distribution model in the cutting zone, a tedious and, in most of the cases, an inaccurate or even contradictory estimation, for the analysis under the desired cutting conditions [Kr 66, Shaw 84].

6. The tool wear and built-up edge are assumed to be insignificant under the cutting conditions applied in this analysis. For example, if the time period for cutting is restricted to be less than a fraction of a minute, the tool wear will become

insignificant [Shaw 84, Tr 91]. On the other hand, if the cutting speed is set high enough, the size of the built-up edge will actually become small and even diminished during machining [Sa 63]. As a justification for these assumptions, the machining tests performed in this work were confined to observe these phenomena.

## 3.2 Modeling of Elastoplastic Deformation in the Cutting Zone

If the effect of plastic flow on the cutting process is to be considered, the material property of the workpiece should include the information beyond the elastic region which is also necessary for the nonlinear stress-strain finite element analysis. The workpiece materials being used in this study are AISI 1020 steel and 6061-T6 aluminum alloy. Based on the available test data [Alloy 75, Bo 87], the true stress-strain relation of an AISI 1020 steel as well as the modulus of elasticity and the Poisson's ratiocan be found. Similar information for 6061-T6 aluminum alloy is also available [Alloy 75, Ha 84].

Since the problem defined in this research involves the large strain analysis of elastoplastic deformation, the governing equations and constitutive laws have to be carefully determined. An *updated Lagrangian* type formulation is chosen for this analysis as it's more suitable for solving this type of problems [Na. 81, CaSt 88].

The incremental approach of the *updated Lagrange* procedure is based on the following concepts (a detail description can be found in [Na. 81]):

1. During each analysis increment a Lagrangian formulation is used; i.e., the state variables are defined with respect to the state at the start of the increment.

2. At the end of each increment, the state variables are *updated* with respect to the state at the end of the increment.

The equilibrium of a body, at the start of the increment, can be expressed by the virtual work equation in a Cartesian coordinate system (for brevity, only surface loads are considered here):

$$\int_V \sigma_{ij}\delta\varepsilon_{ij}dV = \int_S P_i\delta u_i dS \tag{1}$$

where $\sigma_{ij}$ are the Cauchy stresses, $\delta\varepsilon_{ij}$ are the variations in strain, $V$ is the volume of the body, $P_i$ are the surface loads on the body, $\delta u_i$ are the variations in displacement, and $S$ is the surface of the body.

The virtual work (equilibrium) equation when subjected to an increment displacement, $\Delta u_i$, can be derived as

$$\int_V (\Delta S_{ij}\delta_{ki} + S_{ij}\Delta u_{k,i} + \Delta S_{ij}\Delta u_{k,i})\delta u_{k,j}dV = \int_S \Delta P_i\delta u_i dS \tag{2}$$

and

$$\Delta S_{ij} = \mathcal{L}_{ijkl}(\Delta u_{k,l} + \frac{1}{2}\Delta u_{m,k}\Delta u_{m,l}). \tag{3}$$

In the above equations, the $S_{ij}$ are the second Piola-Kirchhoff stresses, and

$$\mathcal{L}_{ijkl} = \mathcal{L}^{e-p}_{ijkl} - \frac{1}{2}(\delta_{ik}\sigma_{ij} + \delta_{jk}\sigma_{il} + \delta_{il}\sigma_{jk} + \delta_{jl}\sigma_{ik}) + \sigma_{ij}\delta_{kl} \tag{4}$$

where $\mathcal{L}_{ijkl}^{e-p}$ are the elastic-plastic moduli for usual small-strain analysis. Equations 2 and 3 are the governing equations need to be solved simultaneously in the procedure. They can be solved by a *strain correction* method [Na. 81].

At the end of the increment, the state variables need to be updated. The second Piola-Kirchhoff stresses must be transformed to true (Cauchy) stresses; i.e.,

$$\sigma_{ij} = (\delta_{ik} + \Delta u_{i,k})(S_{kl} + \Delta S_{kl})(\delta_{jl} + \Delta u_{j,l})/\mathbf{J} \tag{5}$$

where $\mathbf{J}$ is the Jacobian of the deformation increment. The Jocobian will be equal to unity if the large deformations are incompressible in the plastic region, which is usually the case for metal plasticity. If the same assumption applies, the last term in equation 4, a non-symmetric term, can be neglected, which in turn makes the equation symmetric.

When cutting tool moves along the tool path, it forces the undeformed chip to deform. When the plastic strain in the workpiece reaches a critical point, chip separates from the workpiece, and it must involve the fracture at the vicinity around the tool tip [Ox 89]. As a result, the chip and workpiece should be handled separately as this is occuring. A special option called *tying condition* which *ties* the nodes on the undeformed chip and those on the workpiece material is applied for this purpose. Initially, the nodes on the interface of the undeformed chip and workpiece are constrained together in all the degrees of freedom. When a certain separation condition is reached, the constraints just in front of the tool tip are released to allow the nodes on the chip side to separate from those on the workpiece side. On the other hand, when the just formed chip is *adhered* to the rake face of the tool, a new *tying condition* is applied on the tool-chip interface until the strain in the chip is beyond a certain limit, and the *tying condition* on the tool-chip interface is then released. The tool is then moved along the path with a small stepsize to insure the stability and accuracy of the solution.

How does one determine when the chip should separate from the workpiece, and when the chip should separate from the tool? Basically, there are two criteria to apply: the distance tolerance criterion [UsSh 82, Ko. 91], and the critical plastic strain criterion [CaSt 88]. The distance tolerance depends on the size of the element and has to be small enough such that the gap in front of the tool tip and the error on the steady-state response in the calculation are minimum. However, it is difficult to determine a suitable magnitude of the distance tolerance to satisfy the accuracy and stability requirements. In this study, the critical plastic strain criterion is, therefore, used. Based on the stress-strain relation of the material, if the equivalent plastic strain is beyond a critical value, $\epsilon_{cr}$ (e.g., 0.12 for AISI 1020 steel and 0.32 for 6061-T6 aluminum alloy), the material will be fractured [Bo 87]. This critical plastic strain is fixed throughout the study as the criterion to determine the chip separation condition.

### 3.3 Finite Element Solution Phase

A commercially available finite element program is used to perform the solution part of this study [MARC 91]. The program allows contact between solid bodies such as the tool-work interface in this study. The contact option that governs the contact interface prevents penetration of one body into the other as well as sliding with separation when the tool is in contact with the workpiece. The updated Lagrange formulation, as mentioned in

Section 3.2, is also integrated as an option of the plasticity algorithms in this finite element program. The solution phase of the finite element program can be briefly divided into two steps; i.e., 1) the integration of the rate equations to the nonlinear incremental equations, and 2) the solution of the nonlinear incremental equations where a maximum number of 15 iterations are allowed to meet a given convergence criterion as described below.

To guarantee the convergence, the *nodal force equilibrium* criterion is used in this analysis. A prescribed nodal force tolerance ($F_{tol}$) should be a small fraction of the expected force in the solution phase. A value of 10 N is chosen as the tolerance since it is less than 0.5% of the mean values of the force generated in the solution phase. If the convergence (or the stability) of each increment is satisfied, the tool, which is treated as a rigid body in this study, is then *advanced* along the cutting direction by an amount equivalent to a preset increment size ($\Delta Z$) for the next computation cycle. The optimal increment size is determined by preliminary simulations of choosing different quantities between 0.01 and 0.9 times the size in the cutting direction of an element (0.2 *mm* in this study). It is found that when $\Delta Z$ is less than or equal to 0.01 times the element size, the stability and accuracy of the solution are well controlled (i.e., no undesirable interrupts) during the calculation. Based on that, the increment size is fixed at 0.002 *mm* in this study.

The solution phase is stopped when the number of increments reaches a preset number. The stress/strain fields calculated from each increment can be restored as the initial conditions for further analysis if necessary. This provides the flexibility for debugging the calculation in the middle of the analysis since the result from each increment can be checked for accuracy before the next one is proceeded. It is also convenient to recall the stored data file for further calculation if some problems interrupted the previous run in the middle of calculation. The special features and parameters used in this three-dimensional finite element analysis are summarized in Table 1.

Table 1: Special Features and Parameters Used in the Analysis

| | |
|---|---|
| Special Features | Updated Lagrange Formulation, *Tying* Conditions, *Contact* Options. |
| F.E.M. Parameters | $F_{tol}$=10 N, $\Delta Z$=0.002 mm., $\epsilon_{cr}$ = 0.32 for 6061-T6 aluminum alloy, $\epsilon_{cr}$ = 0.12 for AISI 1020 steel |
| Cutting Conditions | Feed Rate = 0.05 through 0.38 mm/rev., Depth of Cut=0.13 through 0.25 mm. |
| Tool Settings | Tool Nose Radius=0.8 mm, Rake Angle=5°, Lead Angle=−5° (for carbon steel), 45° (for aluminum). |

## 3.4 Description of Results from Analysis

Based on the aforementioned procedure used in the finite element analysis, results under different cutting conditions and workpiece materials are available. From the analysis, results such as deformed meshes, equivalent plastic strain ($\epsilon_p^{eq}$) and equivalent *von Mises* stress ($\sigma_M^{eq}$) are obtained. Then, a specially chosen surface quality index is evaluated from the deflections of nodal points on the deformed surface for comparison.

Figure 6 shows the deformed shapes of steel being cut under one cutting condition (as indicated in the figure) at different load steps near the cutting zone. The actually calculated deflections of the chip and workpiece are represented in the figure. The figure only displays a portion of the original finite element meshes since we are interested in the region near the cutting zone in the material being cut. To do so, five *clip planes* (four sides and the bottom one) are applied to the model to *cut out* a portion of the finite element mesh from Fig. 5. The cutting tool is also excluded from Fig. 6 to give a clearer view of the cutting zone.

As can be seen in Figs. 6a to 6d, the deformed shapes yield a qualitative assessment of the expected physical behavior in metal cutting. For example, it can be seen from the time history as shown in Figs. 6a to 6d that the chip is traveling up toward the tool rake face and the shearing process is developing progressively near the tool-work interface region (e.g., the separation of the just-formed chip from the machined surface).

Iso-strain contours of the equivalent plastic strain ($\epsilon_p^{eq}$), corresponding to the deformed shapes under different load steps are displayed in Figs. 7a to 7d as well. Figure 7a is the total picture of the equivalent strain on the model under load step 30 which gives a picture of the range of plastic strain distributed in the material. This information also gives a quantitative assessment of the development of plastic strain as the tool advancing forward. Similarly, iso-stress contours of the equivalent von Mises stress ($\sigma_M^{eq}$) corresponding to the deformed shapes under different load steps are displayed in Figs. 8a to 8 d.

By finding the resultant reaction forces from the nodal points on the tool-work interface, the steady-state cutting forces in the tangential ($z$) and feed ($x$) directions can be estimated from the analysis. Moreover, from the deformed shapes, the deflections of each node on the machined surface can be calculated and compared with those deduced from the turning tests of AISI 1020 carbon steel and 6061-T6 aluminum alloy cut under the same cutting conditions as described in this finite element analysis.

Figure 9a displays a close-up view of a plastically deflected cross section from the machined surface of the AISI 1020 steel along the feed direction. Figure 9b shows the surface profile taken from the machined surface of the 6061-T6 aluminum alloy. In the same Figure, the surface profiles taken from the results of finite element analysis for both steel and aluminum alloy material under the same cutting conditions are also shown. The thinner lines represent the ideal machined surface profile, which is just a duplicate of the cutting tool geometry, if no elastoplastic deformation and tool vibration is occurred on the machined surface. Comparisons between the deformed surface profiles from experimental results and finite element analysis will be discussed in the next section.

# 4 Experimental Verification and Discussion of Results

## 4.1 Experimental Work

Turning of an AISI 1020 steel bar and 6061-T6 aluminum alloy bar with diameter of 76 $mm$ (3 $in$) and length of 102 $mm$ (4 $in$) were performed to verify the developed finite element model for elastoplastic deformation observed on machined surfaces. The machine tool used is a CNC lathe, and the tool inserts are tungsten carbide inserts. As mentioned earlier, the tool vibration, tool wear, and built-up edges, which can alter the machined surface significantly, should be carefully controlled to their minimum levels such that the surface

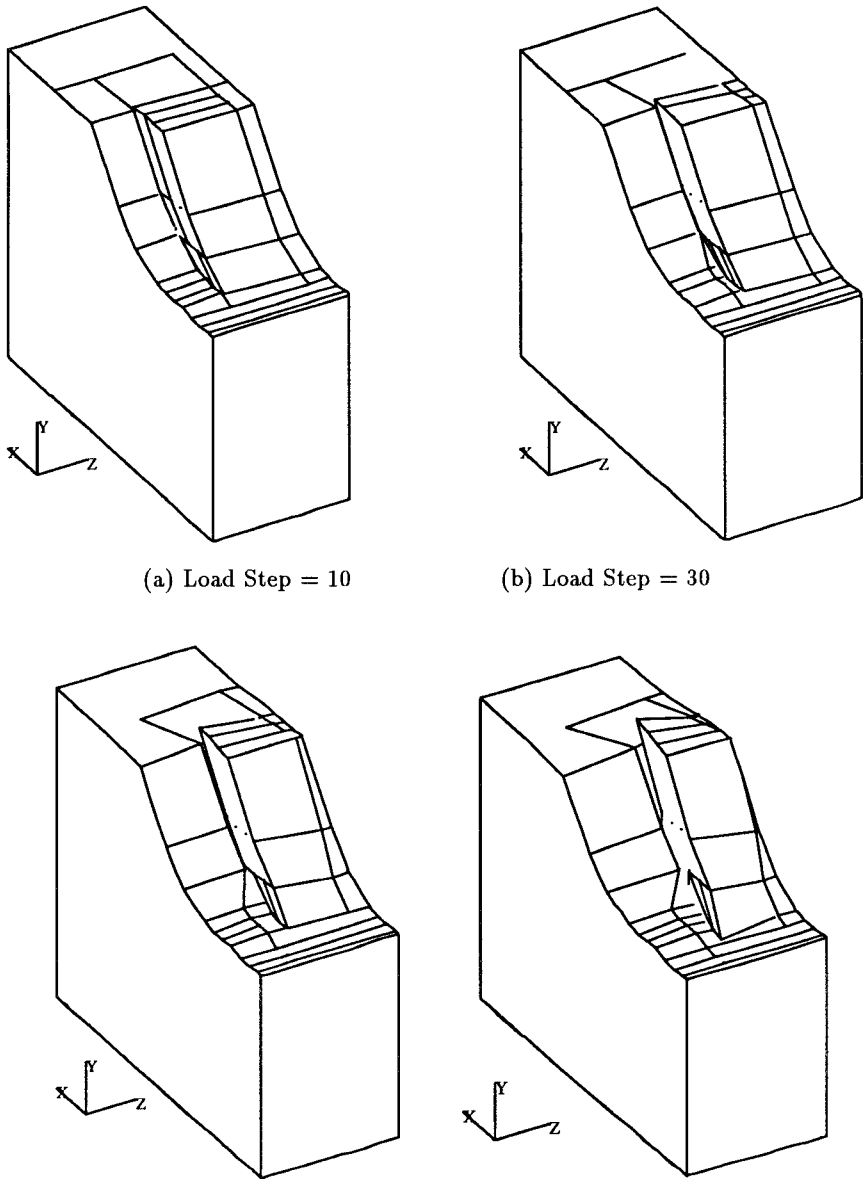


(a) Load Step = 10 (b) Load Step = 30

(c) Load Step = 50 (d) Load Step = 80

Figure 6: Deformed Shapes of Steel at Different Load Step
(Cutting Condition: feed = 0.10 $mm$/rev, depth of cut = 0.25 $mm$)

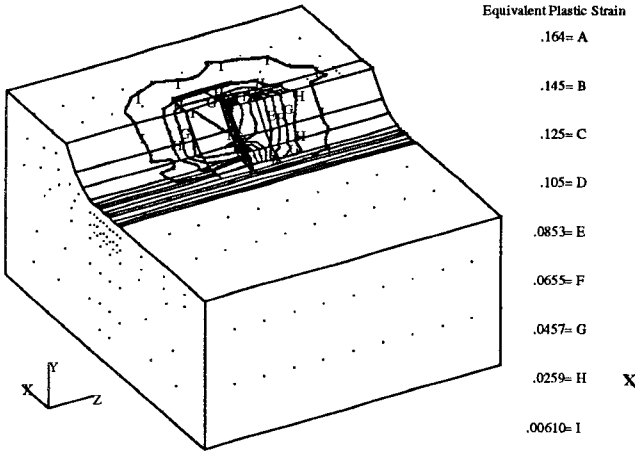


(a) Load Step = 30

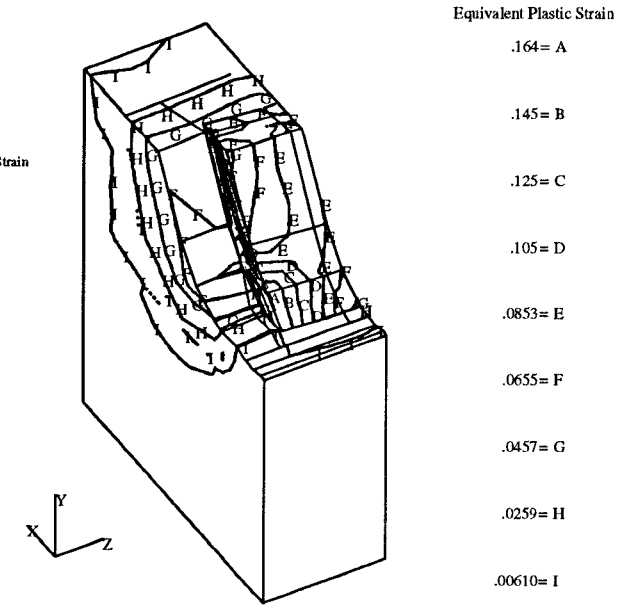


(b) Load Step = 30

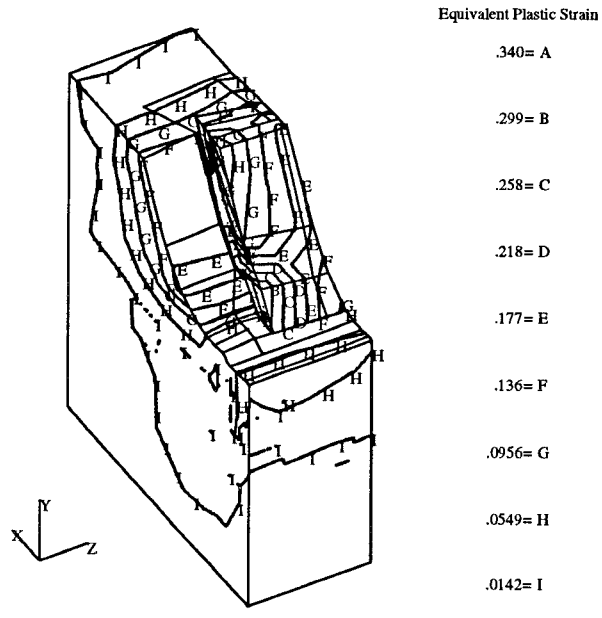


(c) Load Step = 50

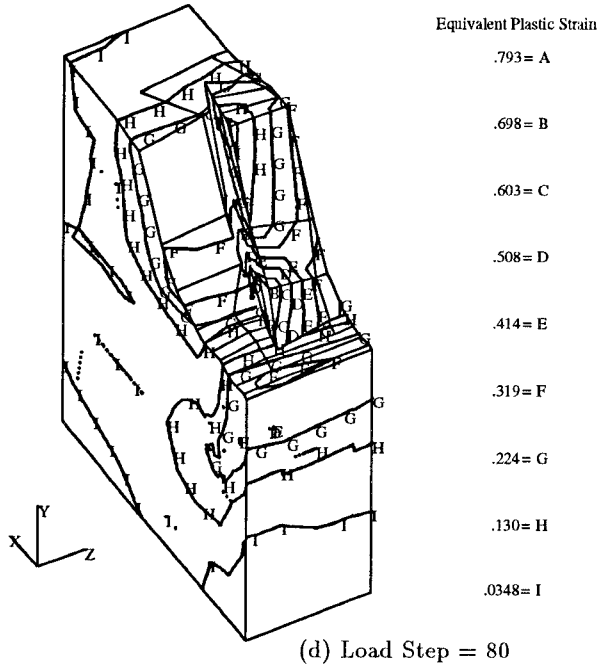


(d) Load Step = 80

Figure 7: Iso-Strain Contours with Deformed Shapes of Steel at Different Load Step (Cutting Condition: feed = 0.10 $mm$, depth of cut = 0.25 $mm$)

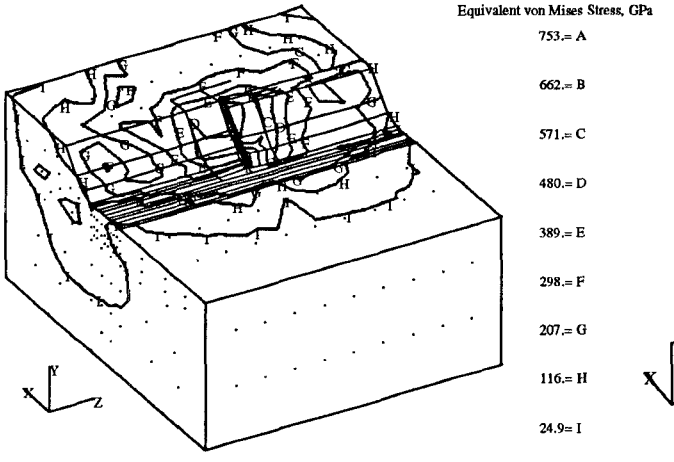


(a) Load Step = 30

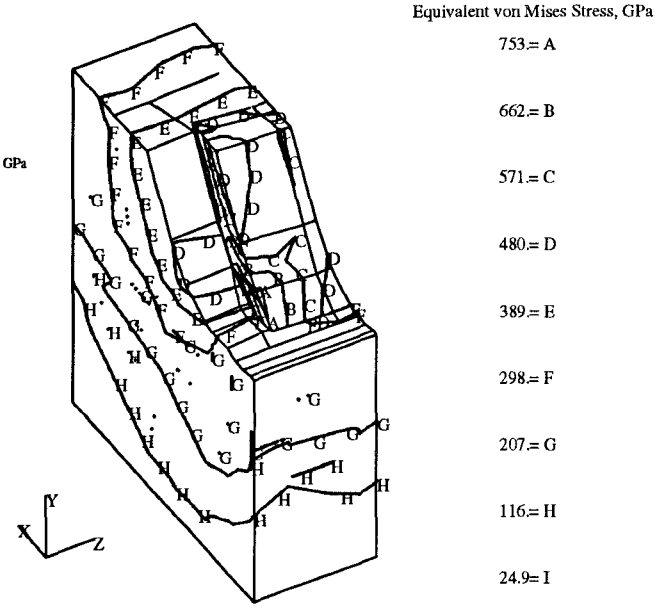


(b) Load Step = 30

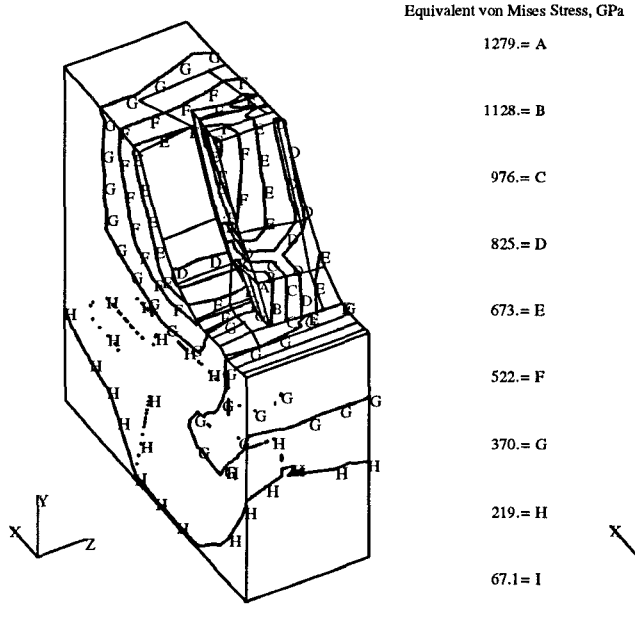


(c) Load Step = 50

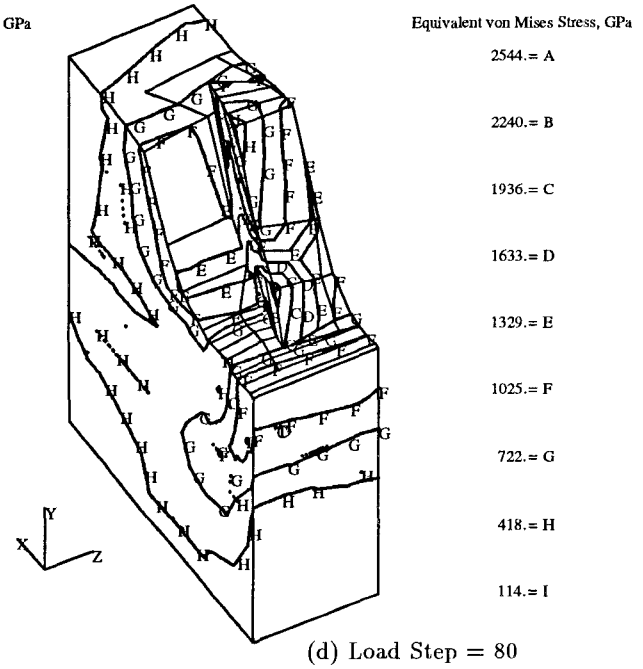


(d) Load Step = 80

Figure 8: Iso-Stress Contours with Deformed Shapes of Steel at Different Load Increment (Cutting Condition: feed = 0.10 $mm$, depth of cut = 0.25 $mm$)

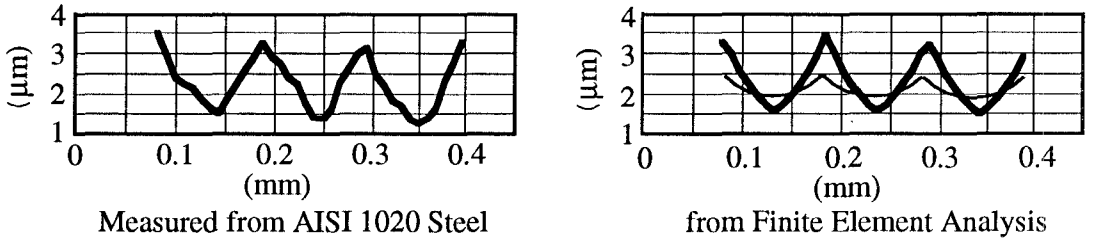


(a) Surface Profiles of AISI 1020 Carbon Steel

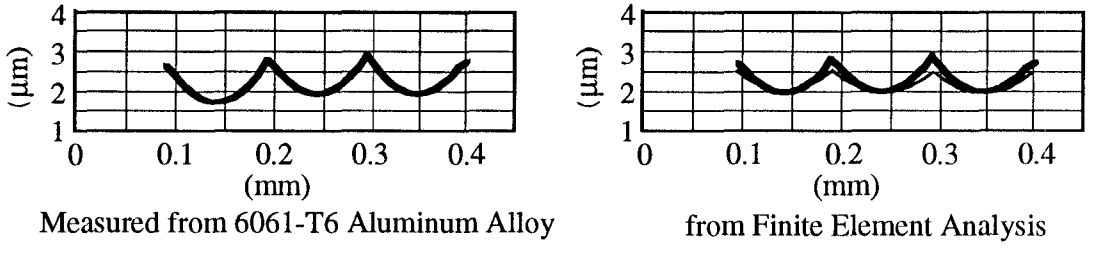


(b) Surface Profiles of 6061-T6 Aluminum Alloy

Figure 9: A Close-up View of the Deflections of Machined Surface Profiles (Cutting Condition: feed = 0.10 $mm$/rev, depth of cut = 0.25 $mm$)

finish due to elastoplastic deformation process during machining tests can be identified and compared with those from the finite element analysis.

As a common practice, the effect due to built-up edges can be reduced by high cutting speed [Sa 63, Shaw 84]. In this study, we choose the spindle speed in the range between 1500 to 1900 *rpm* (360 - 450 surface meter per minute) which is high enough for preventing the built-up edges from occurring on both the steel and aluminum alloy [Shaw 84]. On the other hand, the effect on surface finish due to tool wear can be prevented if each test performed lasts for a very limited time duration. In this study, each cutting test only cuts less than ten seconds and new tool insert is used for each material type.

As for the effect due to tool vibration, it is obvious that the length to diameter ratio of the workpiece (4/3 = 1.33) in this test can provide a very high stiffness between the workpiece and tool during machining. As a result, the vibration during cutting can be reduced significantly compared with those have higher length to diameter ratios. However, the random tool vibration due to material properties can never be suppressed in the cutting tests. To solve this problem, we use a surface index called root mean squared slope or average slope ($dq$). The definition for $dq$ is

$$dq = \sqrt{\frac{\sum_{i=1}^{N} [y_i'(x)]^2}{N}} \tag{6}$$

where $y_i'(x)$ is the derivative of the profile measured from the mean line at the $i^{th}$ sample point along the $x$ direction on which the trace was taken. This index is least sensitive to the tool vibration and most sensitive to the effect of elastoplastic deformation on machined surfaces [Sa 63, Wh. 74]. Therefore, $dq$ will be used as the surface quality index for comparing the results from turning tests and finite element analysis in the following sections.

## 4.2 Effects of Feed Rate, Depth of Cut, and Workpiece Material

### 4.2.1 Feed Rate Effect

Four different feed rates (0.05, 0.1, 0.25 and 0.38 $mm/rev$) are used in the machining tests. Depth of cut is fixed at 0.22 $mm/rev$ (spindle speed is 1500 *rpm* for cutting tests) for each feed rate and applied to the finite element model.

Similar to Fig. 9, the deformed profiles along the feed direction taken from the cutting zone of the finite element model under different feed rates can be evaluated. Moreover, the deflections in the $x$ and $y$ directions of each node are also available from the results of finite element analysis. Based on these deflections, the new coordinates of the nodes on the deformed surface profile and, thus, the average slope of the deformed surface profile can be calculated.

The $dq$'s of both the ideal and deformed surface profiles are calculated based on Eq. 6. The ideal $dq$'s, the calculated $dq$'s from finite element analysis, and those measured from the machined surfaces are shown in Fig. 10a for AISI 1020 carbon steel and Fig. 10b for 6061-T6 aluminum alloy.

The figure shows that the ideal $dq$ linearly increases with the feed rate. It also shows that the $dq$'s measured from machined surfaces possess a similar trend as the feed rate increases. However, there is a big gap in the actual values between the measured and ideal

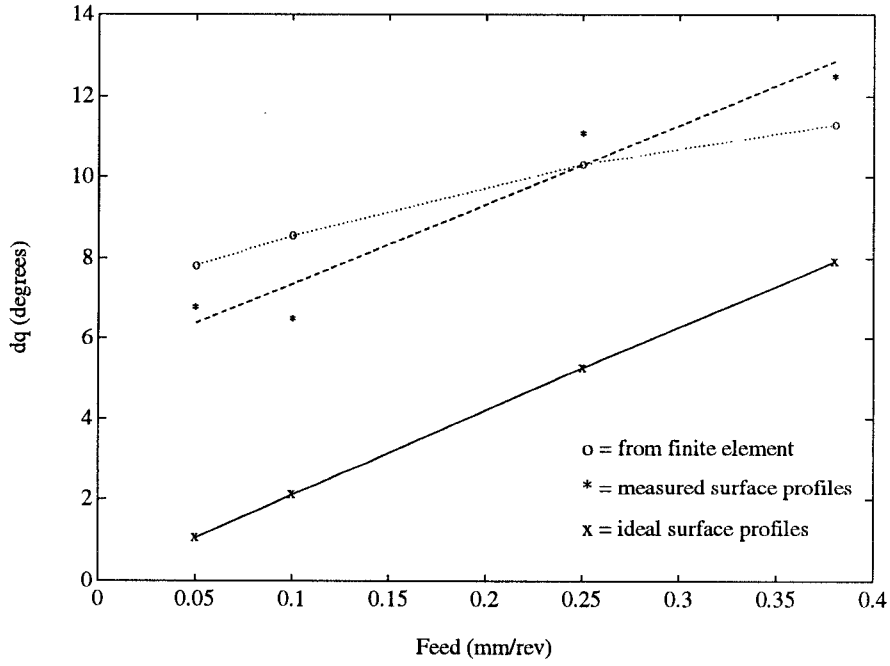


(a) from AISI 1020 Carbon Steel

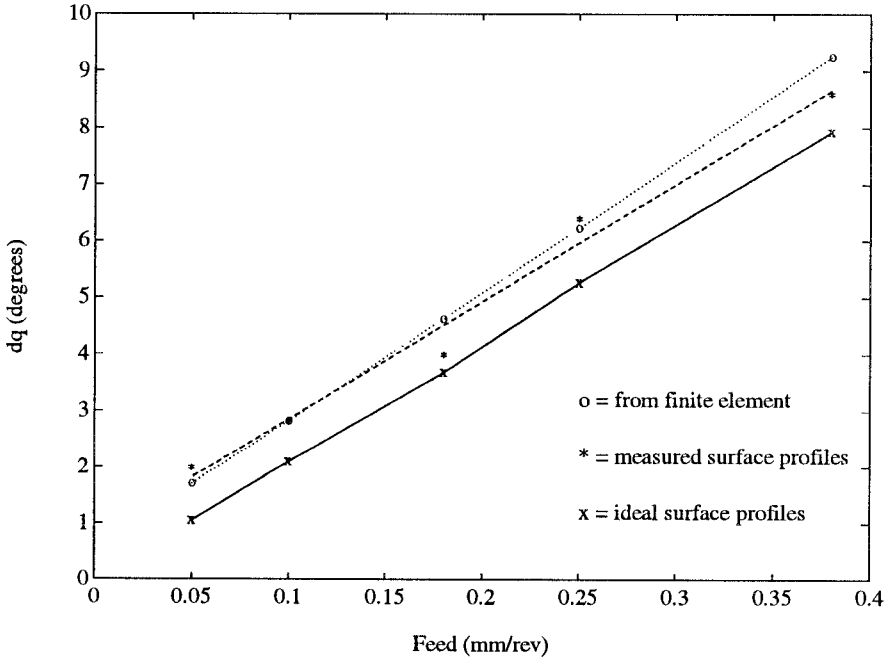


(b) from 6061-T6 Aluminum Alloy

Figure 10: Effect of Feed Rate Change on the Average Slopes ($dq$) of Machined Surfaces

ones. The cause of this gap is mainly from the elastoplastic deformation process occurred on the machined surface during cutting. As shown in the same figure, the estimated $dq$'s from the finite element analyses match with those measured ones. This indicates that the validity of the finite element analysis applied in this study is very promising.

### 4.2.2 Depth of Cut Effect

Comparisons are also made for four different depth of cuts (0.13, 0.15, 0.20 and 0.25 $mm$). Turning tests are carried out under the four depth of cuts. The feed rate is fixed at 0.1 $mm/rev$ (spindle speed is 1900 $rpm$ for cutting tests). Similar to what was discussed for feed rate effect, the average slopes of surface profiles ($dq$) under four depth of cuts can be evaluated from the results of the finite element analyses. Figure 11 shows the ideal average slopes (a constant), the measured average slopes, and the estimated average slopes from the finite element analyses under four depth of cuts for both AISI 1020 carbon steel and 6061-T6 aluminum alloy.

This figure shows that when the depth of cut increases, the average slopes of machined surface profiles reduce, which is opposite to what was observed from the effect of varying the feed rate. This can be explained by the fact that when the depth of cut increases, the cutting force increases more dramatically than that of the increase due to the feed rate change. As a result, the stress and strain distributed on the tool-work interface tend to be so high that most of the material particles under it will sustain the plastical deformation and make the machined surface profile closer to the tool geometrical shape (or the ideal surface profile).

Again, the estimated $dq$'s from the results of finite element analyses match well with the measured ones as can be seen in the figure. This suggests that the finite element model and the analysis approach in this study are necessary to predict the elastoplastic deformation and recovery processes in metal cutting. The predicted average slopes, $dq$'s, are important for the tribological performance of mating parts with relative motions such as bearings, shafts, cylinder bores, brakes, etc. [StDa 84].

### 4.2.3 Effect of Workpiece Material

As can be seen from Figs. 10 and 11, the average slopes of machined surface profiles from both the carbon steel and aluminum alloy are higher than those from the ideal surface profiles. From the same figures, it is also evident that the average slopes of machined surfaces from carbon steel are always higher than those from aluminum alloy. For example, the difference between the measured $dq$'s on steel and those from ideal surface profiles is about five degrees. The difference between those from aluminum alloy and ideal surface profiles is only about one degree.

It can be explained through the properties of different materials. Suppose material $A$ (e.g., carbon steel) possesses higher yield strength and Young's modulus ($E$) than those of material $B$ (e.g., aluminum alloy) as shown in Fig. 12. When the stress exerted by cutting tool in material $A$ reaches the plastic region and is released after the tool moving away, the remaining strain (permanent set) on the machined surface is $d\epsilon_a$. If the material being cut is material $B$, the remaining strain on the machined surface will become $d\epsilon_b$, which is larger than $d\epsilon_a$. This suggests that the elements in material $A$ *recovers* more from the

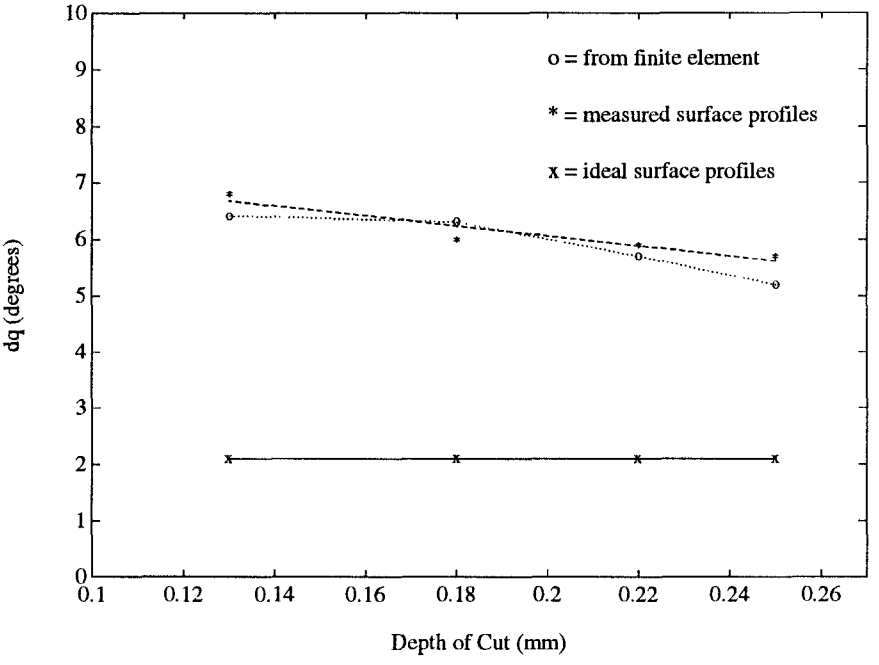


(a) from AISI 1020 Carbon Steel

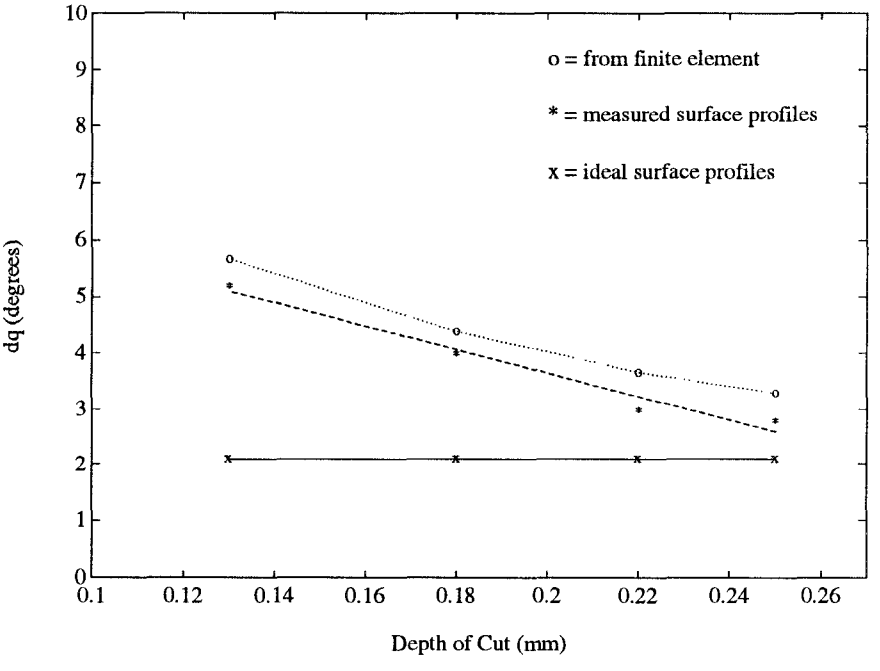


(b) from 6061-T6 Aluminum Alloy

Figure 11: Effect of Depth of Cut on the Average Slopes ($dq$) of Machined Surfaces

plastically deformed state than those from material $B$. As a result, the machined surface profiles of material $A$ will sustain less geometric shape of the cutting tool. This can also be verified by looking at the profiles in Fig. 9a in which the *spring-back* of the profile is more prominent than that in Fig. 9b. From the observation, it can be asserted that the elastoplastic deformation process is more prominent on higher strength materials such as carbon steel than that of lower strength materials such as aluminum alloy.

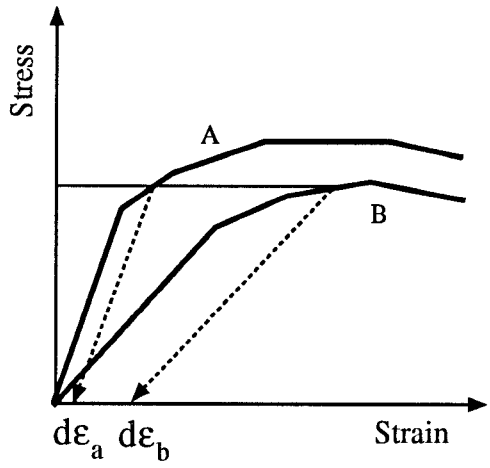


Figure 12: Example of Elastoplastic Deformation and Recovery Processes

### 4.3 Development of a Surface Texture Modification Model

As mentioned in the beginning of this paper, the results from this finite element analysis can be applied as a surface texture modification model to enhance the accuracy of the prediction on machined surface quality.

To develop such a surface texture modification model, the idea is to use the deflections of surface profiles calculated from the results of the finite element analyses for different cutting conditions. For example, given different cutting parameter settings, we can use the finite element models in this study to find the elastically-plastically deformed points along the cutting edge. The estimated deflections on these points can be presented as functions of the cutting parameters (feed rate and depth of cut). As demonstrated in the previous sections, the variation of $dq$'s can be linearly related to the feed rate change or the depth of cut change. Similarly, the functional relations between the deflections on each nodal points along the cutting tool edge and the cutting parameters can be found.

One such example is shown in Fig. 13. The measured surface profile is taken from a machined AISI 1020 steel bar under the same cutting condition as those in Fig. 9. The simulated profile is from a computer-aided surface texture simulator based on the same cutting conditions [ZhHw 90, Hw 92]. The modified profile is based on the results from the finite element analysis. By comparing the three $dq$ values, the measured one (6.5°) and the modified one (6.9°) are very close to each other, while the simulated one (2.7°) is far below the measured one. This example shows that the improvement on $dq$ prediction after the surface texture modification is about 65%. Other cutting conditions are also examined

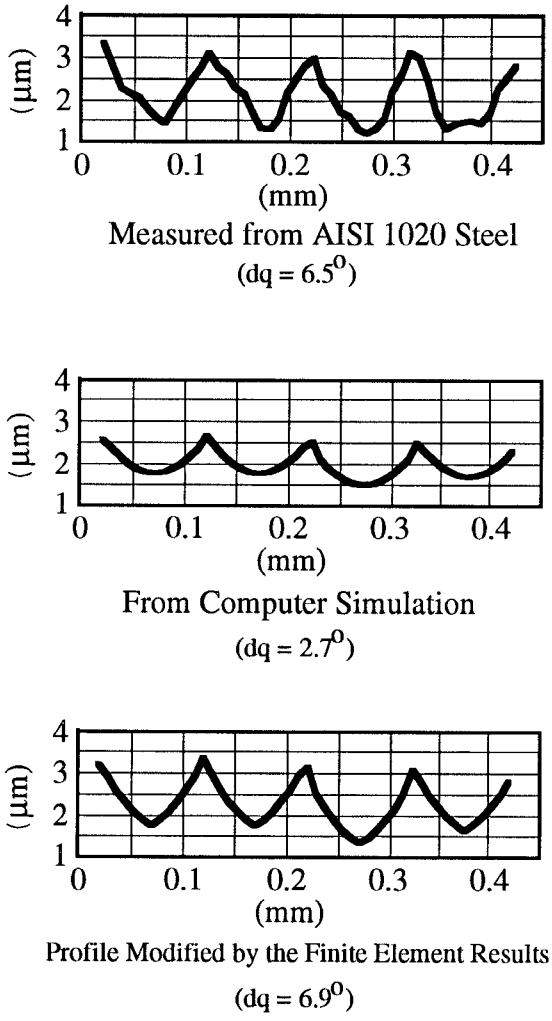


Figure 13: *dq*'s from the Measured, Simulated, and Modified Surface Profiles

after the modification, and the average improvement on the $dq$ prediction is more than 50%. This gives a strong indication that the finite element analysis is a very promising tool for enhancing the accuracy of the computer simulator which can never predict the effect of elastoplastic deformation observed on the machined surfaces.

# 5 Conclusions

In this study, an updated Lagrange approach is applied for analyzing the elastoplastic deformation processes observed on machined surfaces. The emphasis is on investigating the effects of cutting parameters (feed rate, depth of cut, and material property) on the elastoplastic deformation process associated with machining through simulating a single-point cutting process in a three-dimensional space.

The obtained results are in reasonable quantitative agreements with the experimental results when the average slopes of surface profiles ($dq$'s) are compared. It has been shown that the $dq$'s have linear relations with the feed rate as well as the depth of cut (with opposite trends). On the other hand, soft materials (such as aluminum alloy or brass) tend to have less effect of plastic recovery on machined surfaces; thus, the average slopes are smaller and closer to the ideal ones as opposed to the hard materials (such as carbon steel). This phenomenon is also observed from the results of finite element analysis. This enlightens the necessity of applying the results from the finite element analysis as a surface texture modification model. This modification can enhance the accuracy of a surface texture simulator by 50% on predicting the average slopes of machined steel, an important index for tribological performance of mating parts.

The developed finite element model can be extended to account for more complex metal cutting behavior, such as frictions between tool-work or tool-chip interface under *low cutting speed*, effect of built-up edges or tool wear phenomenon. It could also be applied to the study of machining of non-metallic materials such as advanced ceramics.


## Acknowledgements

The authors acknowledge the support of the University General Research Board, the Department of Mechanical Engineering, and the Institute for Systems Research at the University of Maryland at College Park under Engineering Research Centers Program: NSFD CDF 8803012.


# References


[Alloy 75] Alloy Digest, Engineering Alloys Digest, Inc., Upper Montclair, New Jersey, 1975.

[BoTa 54] Bowden, F.P. and Tabor, D., Friction and Lubrication of Solids, Oxford University Press, 1954.

[Bo 87] Boyer, H.E. (editor), Atlas of Stress-Strain Curve, American Society of Metals, 1987.

[CaSt 88] Carroll, J.T. and Strenkowski, J.S., *Finite Element Models of Orthogonal Cutting with Application to Single Point Diamond Turning*, Int. J. Mech. Sci., vol. 30, no. 12, pp. 899-920, 1988.

[ErMe 41] Ernst, H. and Merchant, M.E., *Chip Formation, Friction, and Finish*, Cincinnati Milling Machine Company, Cincinnati, Ohio, 1941.

[Ha 84] Hatch, J.E. (editor), Aluminum : Properties and Physical Metallurgy, American Society for Metals, 1984.

[Hw 92] Hwang, T.W., Analysis of Surface Quality in Machining of Metals and Advanced Ceramics, Ph. D. dissertation, Univeristy of Maryland at College Park, 1992.

[Iw. 84] Iwata, K., Osakada, k. and Terasaka, Y., *Process Modeling of Orthogonal Cutting by the Rigid-Plastic Finite Element Method*, ASME Journal of Engineering Materials and Technology, vol. 106, pp. 132-138, 1984.

[Kl 73] Klamecki, B.E., *Incipient Chip Formation in Metal Cutting-A Three Dimensional Finite Element Analysis*, Ph.D. dissertation, University of Illinois at Urbana Champaign, 1973.

[Ko. 91] Komvopoulos, K. and Erpenbeck, S.A., *Finite element Modeling of Orthogonal Metal Cutting*, ASME Journal of Engineering for Industry, vol. 113, pp. 253-267, 1991.

[Kr 66] Kronenberg, M, Machining Science and Application - Theory and Practice for Operation and Development of Machining Processes, Pergamon Press, Inc., 1966.

[Lin 91] Lin, Zone-Ching, Lin, Yau-Yi and Liu, C.R., *Effect of Thermal Load and Mechanical Load on the Residual Stress of Machined Workpiece*, Int. J. Mech. Sci., vol. 22, no. 4, pp. 263-278, 1991.

[MARC 91] MARC K.4 Users Manual, Vol. A, MARC Analysis Research Corp., Palo Alto, California, 1991.

[Na. 81] Nagtegaal, J.C. and de Jong, J.E., *Some Computational Aspects of Elastic-Plastic Large Strain Analysis*, Int. J. Num. Meth. Engng., vol. 17, pp. 15-41, 1981.

[Ox 89] Oxley, P.L.B., Mechanics of Machining - an analytical approach to assessing machinability, John Wiley & Sons, 1989.

[Sa 63] Sata, T., *Surface Finish in Metal Cutting*, CIRP Annalen, XII, 1963, pp. 190-197.

[Shaw 84] Shaw, Milton C., Metal Cutting Principles, Oxford University Press, N. Y., 1984.

[St. 83] Stevenson, M.G., Wright, P.K. and Chow, J.G., *Further Developments in Applying the Finite Element Method to the Calculation of Temperature Distributions in Machining and Comparisons with Experiment*, ASME Journal of Engineering for Industry, vol. 105, pp.149-154, 1983.

[StDa 84] Stout, K. J. and Davis, E. J., *Surface Topography of Cylinder Bores: the Relationship between Manufacture Characterization and Function*, Wear, Volume 95, 1984, pp. 111-125.

[StCa 85] Strenkowski, J.S. and Carroll, J.T., *A Finite Element Model of Orthogonal Metal Cutting*, ASME Journal of Engineering for Industry, vol. 107, pp. 349-354, 1985.

[Ta. 74] Tay, A.O., Stevenson, M.G. and Davis, G.D.V., *Using the Finite Element Method to Determine Temperature Distributions in Orthogonal Machining*, Proc. Inst. Mech. Engrs., 188, pp. 627-638, 1974.

[TlAn 83] Tlusty, J., and Andrews, G.C., *A Critical Review of Sensors for Unmanned Machining*, Annals of the CIRP, vol.32/2/1983, pp. 563-572.

[Tr 91] Trent, E.M., Metal Cutting, 3rd ed., Butterworth Heinemann, Oxford, 1991.

[UsSh 82] Usui, E. and Shirakashi, T., *Mechanics of Machining - From "Descriptive" to "Predictive" Theory*, On the Art of Cutting Metals-75 Years Later, ASME PED vol.7, pp. 13-35, 1982.

[Wh. 74] Whitehouse, D. J., Vanherck, P., deBruin, W., and van Luttrervelt, C. A., *Assessment of Surface Typology Analysis Techniques in Turning*, Annals of the CIRP, Vol. 23/2, pp. 265-282, 1974.

[ZhHw 90] Zhang, G.M. and Hwang, T.W., *Analysis of the Cutting Dynamics in Microscale*, PED - Vol. 43, 1990 ASME Winter Annual Meeting, pp. 25-37, 1990.

[ZiGo 74] Zienkiewicz, O.C. and Godbole, P.N., *Flow of Plastic and Visco-Plastic Solids with Special Reference to Extrusion and Forming Processes*, Int. J. Num. Meth. Engng., vol. 8, pp. 3-16, 1974.